computation

MDPI

Article

Finite Element Analysis of Occupant Risk in Vehicular Impacts into Cluster Mailboxes

Emre Palta [1], Lukasz Pachocki [2], Dawid Bruski [2], Qian Wang [3], Christopher Jaus [4] and Howie Fang [4,*]

[1] Department of Mechanical Engineering, Tekirdag Namik Kemal University, Tekirdag 59030, Turkey; epalta@nku.edu.tr
[2] Department of Mechanics of Materials and Structures, Faculty of Civil and Environmental Engineering, Gdansk University of Technology, 80-222 Gdansk, Poland; lukpacho@pg.edu.pl (L.P.); dawbrusk@pg.edu.pl (D.B.)
[3] Department of Civil and Environmental Engineering, Manhattan University, Riverdale, NY 10471, USA; qian.wang@manhattan.edu
[4] Department of Mechanical Engineering, Liberty University, Lynchburg, VA 24515, USA; ckjaus@liberty.edu
* Correspondence: hfang@liberty.edu; Tel.: +1-(434)-582-7859

Abstract: The deployment of cluster mailboxes (CMs) in the U.S. has raised safety concerns for passengers in potential vehicular crashes involving CMs. This study investigated the crashworthiness of two types of CMs through nonlinear finite element simulations. Two configurations of CM arrangements were considered: a single- and a dual-unit setup. These CM designs were tested on flat-road conditions with and without a curb. A 2010 Toyota Yaris and a 2006 Ford F250, both in compliance with the Manual for Assessing Safety Hardware (MASH), were employed in the analysis. The simulations incorporated airbag models, seatbelt restraint systems, and a Hybrid III 50th percentile adult male dummy. The investigations focused on evaluating the safety of vehicle occupants in 32 impact scenarios and under MASH Test Level 1 conditions (with an impact speed of 50 km/h). The simulation results provided insights into occupant risk and determined the primary failure mode of the CMs. No components of the mailboxes were found intruding into the vehicle's occupant compartment. For all considered cases, the safety factors remained within allowable limits, indicating only a marginal risk of potential injury to occupants posed by the considered CMs.

Keywords: cluster mailbox (CM); finite element analysis; vehicular crash; transportation safety; occupant safety

Academic Editors: Anna T. Lawniczak, Andrés Amador Garcia-Granada and Hirpa G. Lemu

Received: 31 October 2024
Revised: 23 December 2024
Accepted: 3 January 2025
Published: 8 January 2025

Citation: Palta, E.; Pachocki, L.; Bruski, D.; Wang, Q.; Jaus, C.; Fang, H. Finite Element Analysis of Occupant Risk in Vehicular Impacts into Cluster Mailboxes. *Computation* **2025**, *13*, 12. https://doi.org/10.3390/computation13010012

1. Introduction

Cluster mailboxes (CMs) are increasingly used to replace traditional single-family mailboxes in newly developed neighborhoods in the United States. The increased number of CMs raises safety concerns for passengers in potential vehicular crashes involving CMs. Most CMs are made of aluminum, available in different sizes and often installed together in a mailbox hub. Although CMs are usually placed in communities where speed limits are generally low, collisions involving passenger vehicles may still lead to serious injuries or even fatalities. Given the increasing presence of CMs, assessing occupant safety during vehicle–CM collisions was deemed essential by transportation safety officials and engineers. To address these concerns, occupant safety during vehicular crashes into CMs was evaluated in this study, following the guidelines and procedures established by the Manual for Assessing Safety Hardware (MASH) [1]. This study aims to contribute to the

understanding of risks associated with these structures and help with informed strategies to enhance roadway safety.

Studies on mailbox crashworthiness have been conducted over a few decades. In the late 1970s, Ross et al. [2] carried out physical crash tests of rural mailboxes using a 1972 Chevrolet Vegas at 96.6 km/h. The mailboxes had one to four box installations with wood and steel posts. A critical part of safety evaluation in the study was on the intrusion of mailbox mounting plates into the occupant compartment through the windshield. In the subsequent full-scale crash tests by Hall and Ross [3], the effect of mailbox supports, embedment depths, and initial impact locations was studied. Campise and Ross [4] evaluated the responses of a CM composed of twelve to sixteen boxes in a metal frame and supported by a single post anchored to a concrete footing. Under the impact of a 1978 Honda Civic at 100.2 km/h, the CM failed to pass the safety criteria defined by Report 230 of the National Cooperative Highway Research Program (NCHRP) due to the vehicle rolling over. Faller et al. [5] performed four crash tests involving various mailbox mounting systems, box configurations, and initial impact speeds using a 1979 Volkswagen Rabbit. Test outcomes demonstrated compliance with the safety criteria outlined in NCHRP Report 230 regarding impact severity. Ross et al. [6] performed multiple physical crash tests to investigate the impact responses of mailbox brackets of a steel, vandal-proof mailbox mounted on a winged channel post. It was found that during high-speed impacts, the mailbox penetrated the occupant's compartment.

Over the past 30 years, numerical simulations have been increasingly used to analyze various problems in the field of transportation safety [7,8], such as the crashworthiness of various roadway safety features [9] and design optimization of safety infrastructures [10–12]. Numerical simulations were also used to evaluate non-standard device installation configurations and to assist road accident reconstructions. For example, Paulsen et al. [13] evaluated a breakaway base for CMs under various impact conditions using finite element (FE) simulations in LS-DYNA [14,15]. The study showed that the CMs met the evaluation criteria outlined in NCHRP Report 350, with a limitation on their inability to establish the extent of risk regarding intrusions into the occupant compartment. Vogel et al. [16] conducted research on mailbox posts and found out that round pipes, square tubing, and U-channels could maintain crashworthiness in line with NCHRP Report 350 evaluation criteria. Tahan et al. [17] studied methodologies to secure mailboxes that were larger and heavier than standard ones. In their investigation, twenty-four impact scenarios were selected for both full-scale crash testing and FE simulations. Both the tests and simulations showed one particularly dangerous case in which the windshield of the striking vehicle, a Geo Metro, was struck by the mailbox component.

In 2006, Sheikh et al. [18] conducted two physical crash tests to study a multi-mailbox mounting system. In these tests, the mailbox anchor was detached from the base when impacted by a 1995 Geo Metro at 35.6 km/h; it hit the vehicle's front bumper and hood and was dragged along by the vehicle. Bligh and Menges [19] assessed the dual- and multi-unit CMs using two physical crash tests based on the Test Level 3 (TL-3) requirements of NCHRP Report 350. Bligh et al. [20] also tested the crashworthiness of three different posts for molded plastic mailboxes: a 4 × 4 wood post, a U-channel, and a 3-inch diameter pipe. They conducted crash tests using the 820C test vehicle specified in NCHRP Report 350 (i.e., a small passenger car with a weight of 820 kg) and found that the upper mailbox unit detached from the lower base during collision and hit the vehicle's hood and windshield. However, there was no observed risk of mailbox intrusion into the vehicle's occupant compartment. Dobrovolny et al. [21] tested and evaluated several CM supports for their crashworthiness when used in locking architectural mailboxes. They found that

larger and heavier mailboxes failed to meet the MASH criteria due to vehicle windshield deformation and intrusions.

Evaluating occupant safety during vehicular crashes often involves the use of anthropomorphic test devices, also known as dummies, in standardized crash tests. Since their first usage in 1976, Hybrid III dummies of various sizes, such as a 50-percentile adult male, a 50-percentile adult female, and children of different ages, have been developed and employed in crash testing. A detailed FE model of the Hybrid III dummy was developed by Noureddine et al. in 2002 [22], whose important contribution was on model validation using actual dummy test results. This validated dummy model entailed improved accuracy on the assessment of dummy responses and the evaluation of potential occupant injuries in vehicular crashes [23,24].

Currently, research on the crashworthiness of CMs is still limited. The mailboxes used in most of the studies only consisted of a mounting post and regular boxes, and no occupant models were included to predict potential safety risks. This study focused on evaluating potential risks to vehicular occupants in collisions with two types of CMs designed by Florence Corporation and approved by the United States Postal Service (USPS) [25]. Finite element simulations, which included a crash test dummy, were conducted to evaluate the CMs under MASH Test Level 1 (TL-1) conditions. The two test vehicle models utilized in crash simulations were MASH-compliant and featured airbags, seatbelt, and a Hybrid III 50th percentile adult male dummy. In the remaining portion of this paper, the FE models of vehicles and CMs are first introduced along with simulation setup and evaluation criteria. Simulation results are then presented and discussed in detail for the two types of CMs, followed by some concluding remarks on research findings.

2. Finite Element Modeling of Vehicles and CMs

2.1. MASH-Compliant Test Vehicles

The two test vehicles used in the FE simulations of vehicular crashes into the CMs were a 2010 Toyota Yaris passenger car (1100C) and a 2006 Ford F250 pickup truck (2270P). The FE models of both test vehicles included seatbelts, airbags, and a Hybrid III crash test dummy to evaluate the risk of occupant injuries. The two test vehicle models are shown in Figure 1.

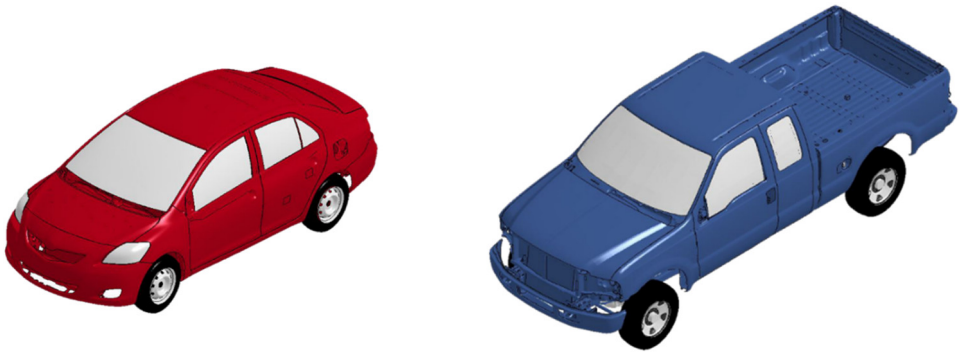

(**a**) (**b**)

Figure 1. FE models of MASH-compliant test vehicles: (**a**) A 2010 Toyota Yaris passenger car (1100C) and (**b**) a 2006 Ford F250 pickup truck (2270P).

The Toyota Yaris model was originally developed and validated against full-frontal, offset-frontal, and side impact tests conducted at the National Crash Analysis Center (NCAC) [26,27]. These models were subsequently modified to improve their numerical accuracy and stability [28–30]. The FE model had a total of 926 components,

602,106 nodes, and 582,681 elements (including 15,156 solid, 562,821 shell, 4685 beam, and 19 discrete elements). The Ford F250 FE model was created at NCAC and validated against NHTSA's frontal-impact test (Test No. 5820) [31]. This model consisted of 746 components, 737,986 nodes, and 735,895 elements (including 25,905 solid, 707,656 shell, 2305 beam, and 29 discrete elements). The Ford F250 model was further improved by eliminating initial penetrations and updating contact definitions to increase model fidelity and numerical stability [32].

2.2. Airbags and Seatbelts

The airbag and seatbelt systems in the vehicle models were modeled in detail to ensure accurate representation of occupant protection mechanisms during crash simulations. The airbag systems were modeled using LS-DYNA's *SECTION_SHELL with ELFORM 9, a fully integrated Belytschko–Tsay membrane formulation. This element type was chosen for its capability of handling large deformations. The airbag membrane had a thickness of 0.35 mm to replicate the behavior of real-life airbag materials under deployment and interaction conditions. The material properties were defined using *MAT_FABRIC (MAT_034) in LS-DYNA. The fabric material had a density of 907.18 kg/m^3, Young's modulus of 100 MPa, Poisson's ratio of 0.4, and shear modulus of 5 MPa. Additionally, Rayleigh damping with a coefficient of 0.05 was adopted, corresponding to 5% of critical damping, to account for energy dissipation during dynamic events.

The airbag deployment in Toyota Yaris was simulated using the Wang–Nefske airbag model [33]. This model utilized a time–history curve to define the inflating gas' mass flow rate (Figure 2), ensuring accurate inflation dynamics. Air leakage during deployment was incorporated through a pressure–volume outflow relationship, accounting for flow blockage due to contact with the dummy and vehicle surfaces. The Ford F250 airbag was modeled using a control volume approach, with the mass flow rate derived from tank tests conducted by NHTSA on a similar system [34].

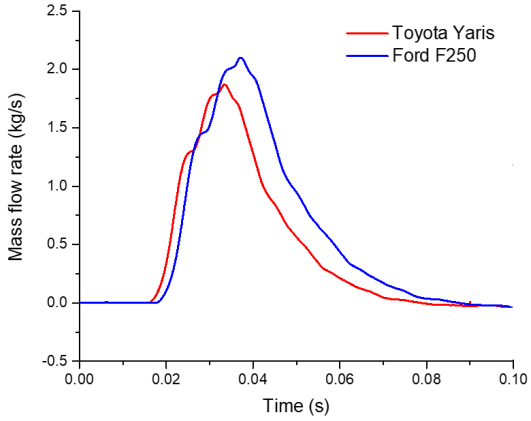

Figure 2. Mass flow rate for the airbags of the two test vehicles.

The seatbelts in both vehicle models were modeled as three-point restraint systems to ensure proper interaction with the dummy's body during crash simulations. The seatbelt webbing was modeled using shell elements defined by *SECTION_SHELL with ELFORM 9, a fully integrated Belytschko–Tsay membrane formulation. To accurately capture the mechanical behavior of seatbelt webbing, the LS-DYNA's *MAT_FABRIC model was adopted with the following material properties: a density of 907.18 kg/m^3, Young's modulus of 2 MPa, Poisson's ratio of 0.3, and a shear modulus of 0.76 MPa. Rayleigh damping with a coefficient of 0.1 was adopted, corresponding to a 10% critical damping to account for energy dissipation.

The D-ring of the seatbelt system was modeled using *ELEMENT_SEATBELT_SLIPRING, allowing the belt to slide freely and adjust during dynamic motion. The retractor was modeled using *ELEMENT_SEATBELT_RETRACTOR, simulating the belt's locking mechanism under high-velocity loads. Pre-tensioning and load-limiting effects were incorporated within the retractor's force–displacement curve [14,15,34], accurately representing the seatbelt's dynamic performance. Detailed modeling and validation work of the airbags and seatbelts can be found in the work by Li et al. [32].

2.3. Hybrid III Crash Test Dummy

The 50th percentile Hybrid III male dummy, as shown in Figure 3, weighed 79.86 kg in the FE model. This dummy model was initially developed by the Livermore Software Technology Corporation, Livermore, CA, USA; it had a total of 349 components, 228,706 nodes, and 338,506 elements (including 186,808 solid, 151,455 shell, 242 beam, and 1 discrete element). Accelerometers were defined in the dummy model at the head, chest, spine, abdomen cavity, pelvis, knees, and ankles to collect acceleration data for safety evaluation. This crash test dummy was positioned into the two vehicles used in this study (see Section 2.1) following NHTSA's guidelines for crash testing, which stipulated that the right and left hands of the dummy be placed on the steering wheel.

Figure 3. FE model of a 50th percentile Hybrid III male dummy.

2.4. Cluster Mailboxes (CMs)

Two distinct types of CMs, Type I and Type IV [35,36], were examined in this study to evaluate their crashworthiness. Both types of CMs, which could be used in single- and dual-unit configurations, were fabricated from 6061-T6 aluminum alloys with powder coat finishes for enhanced durability and corrosion resistance. The single-unit Type I CM was 770 mm in width, 460 mm in depth, and 1570 mm in total height. The upper body was supported by a 720 mm long pedestal column with a rectangular cross-section of 102 mm × 137 mm (4 inches × 5.41 inches) and a wall thickness of 2 mm. The single-unit Type IV CM had the same width and depth as Type I CM but a taller upper body and thus a shorter pedestal column (370 mm) to maintain the same total height as Type I CM. The pedestal base for both types of CMs was a square plate of 305 mm × 305 mm with a thickness of 12 mm. Bolt hole spacings on the pedestal base were 254 mm along the width and 102 mm along the depth. The dual-unit configurations consisted of two mailboxes placed side by side with a 76 mm (3-inch) gap, as illustrated in Figure 4.

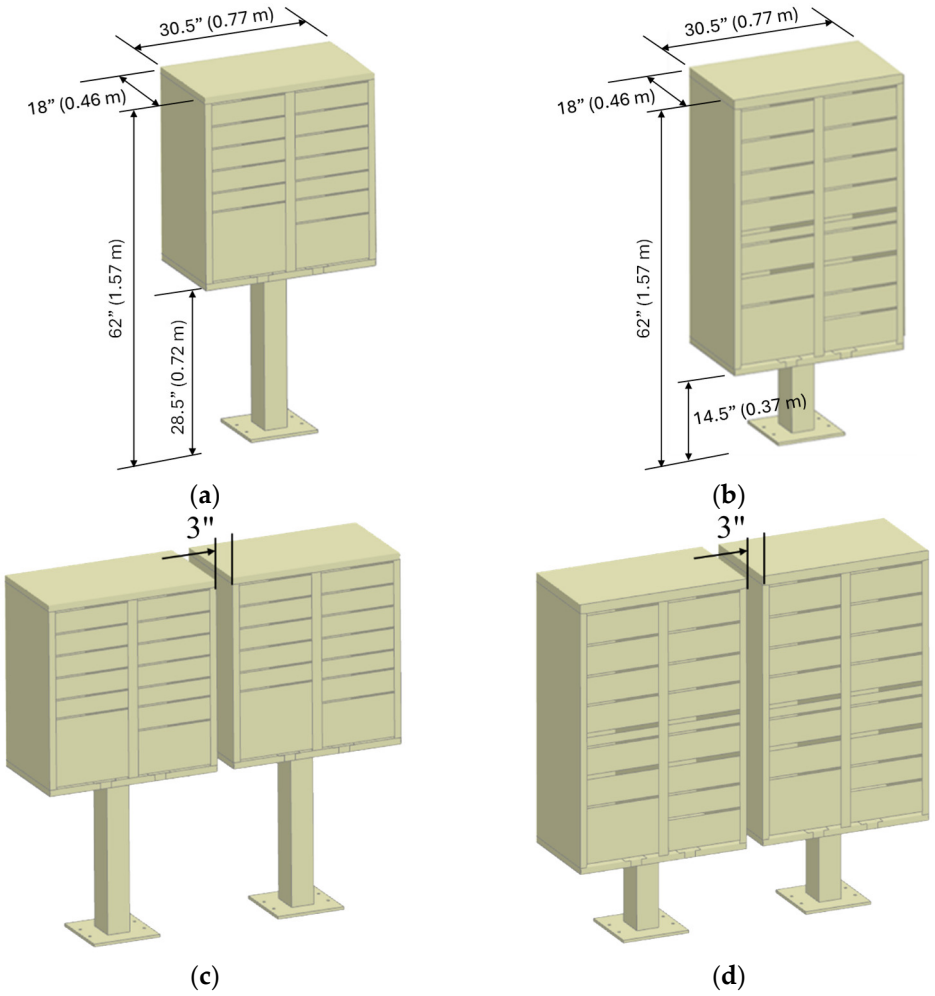

Figure 4. FE models of single- and dual-unit Type I and Type IV CMs. (**a**) Single-unit Type I; (**b**) single-unit Type IV; (**c**) dual-unit Type I; and (**d**) dual-unit Type IV.

The mailbox components were discretized using both shell and solid elements in LS-DYNA. The outer surfaces of the mailbox were modeled using Belytschko–Tsay shell elements (ELFORM 16) with a thickness of 3 mm, while the mail slots were assigned to a thickness of 2.5 mm. The Belytschko–Tsay shell element formulation was chosen for its computational efficiency and robust performance in impact simulations, offering a good balance between accuracy and computational cost. A mesh size of approximately 7 mm was used for the shell elements to adequately capture the deformation behavior while maintaining reasonable computation times. For the pedestal and its base, constant stress solid elements (ELFORM 1) were employed with an approximate element size of 4 mm. This element formulation, which is the default in LS-DYNA, uses single-point integration with hourglass control and is particularly suitable for modeling thick structures under impact loading conditions. To prevent potential hourglass modes, type 4 hourglass control (Flanagan–Belytschko stiffness form) was applied to the solid elements with an hourglass coefficient of 0.1. The single-unit Type I CM model consisted of more than 322,000 elements, while the Type IV model, featuring a shorter pedestal height, comprised over 260,000 elements.

The material model of CM components was *PLASTIC_KINEMATIC (MAT_003) in LS-DYNA to simulate their dynamic response under impact scenarios. The Al 6061-T6 alloy had a density of 2700 kg/m^3, Young's modulus of 68.9 GPa, Poisson's ratio of 0.33, yield strength of 276 MPa, and tangent modulus of 700 MPa. The model employed a

bilinear stress–strain relationship with linear strain hardening to describe the material's elasto-plastic behavior. To account for strain-rate effects, the default yield stress scaling formulation (VP = 0.0) was utilized, enhancing the model's ability to replicate aluminum's performance under high strain-rate conditions. Element erosion was adopted with a failure strain of 0.5 to allow for element deletions when exceeding this strain threshold, effectively capturing material failure during high-energy impacts. This material formulation provided a computationally efficient yet robust representation of the aluminum components' mechanical behavior under impact loading.

The connection between the pedestal column and top plate was modeled using bolt-and-nut assemblies (see Figure 5) that were designed to comply with USPS proprietary specifications. The assembly employed 10-32 UNC bolts (4.8 mm diameter) paired with lock nuts. The bolt and nut geometries were discretized using solid elements (ELFORM 1), ensuring accurate representation of their physical dimensions. The load transfer and connection behavior were simulated using a discrete element (*ELEMENT_DISCRETE) to connect the bolt head to the nut. This discrete element incorporated a nonlinear elastic spring property (*MAT_SPRING_NONLINEAR_ELASTIC) to replicate the bolt's load–displacement response under dynamic loading conditions. A translational spring option (DRO = 0) and a failure displacement criterion (FD) of 0.5 were adopted to capture potential bolt failure during impact.

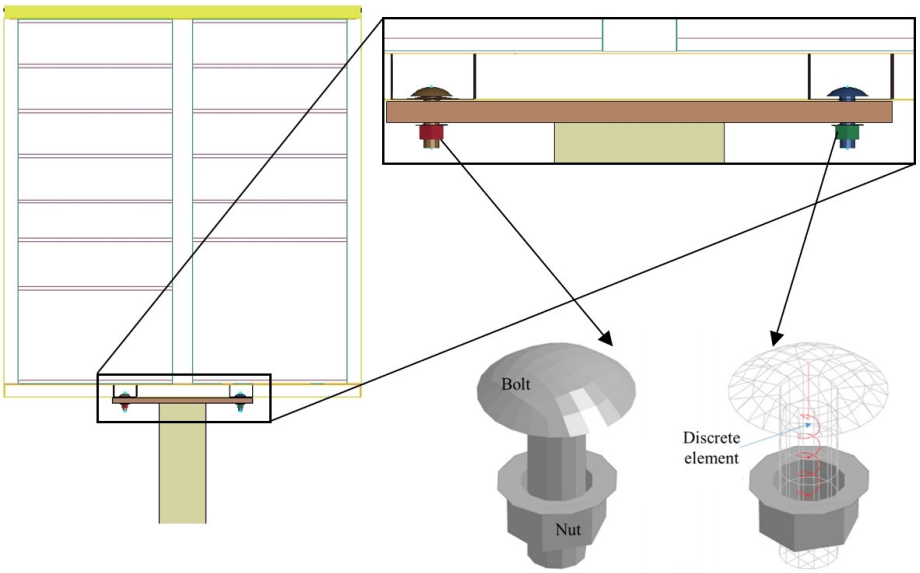

Figure 5. FE model of the bolt and nut.

To simulate the clamping force, an initial elongation was applied to the discrete element, effectively preloading the bolt. The contact between the bolt shank and the holes in the pedestal and horizontal beams was modeled using *CONTACT_AUTOMATIC_SURFACE_TO_SURFACE, with a friction coefficient of 0.2 to allow for sliding movements during dynamic events. To prevent spurious failure of the bolt assembly, the bolt head and nut nodes were constrained using *CONSTRAINED_NODAL_RIGID_BODY, maintaining the structural integrity of the connection. The pedestal base plate was anchored to the ground using *BOUNDARY_SPC_SET with all degrees of freedom fixed, simulating a rigidly secured support. This approach ensured accurate simulation of the bolt-and-nut assemblies' mechanical performance and potential failure modes during impact scenarios.

2.5. Road Surfaces

The CMs were evaluated on two different road configurations: a flat road and a road with a curb. The flat road was represented as a 4-node shell element, while the road with a curb was modeled with two flat surfaces joined by a curb measuring 127 mm in height. Both road surfaces were defined using a rigid material model to ensure realistic interaction with the vehicles during the crash simulations. The road models had overall dimensions of 40,000 mm in length and 7812 mm in width. In simulations involving the curb, the CMs were positioned 2440 mm (8 feet) behind the curb face (i.e., the vertical surface). These configurations facilitated a comparative assessment of the mailbox performance under varying road conditions. Figure 6 provides an overview of the finite element representations of both road types utilized in the analysis.

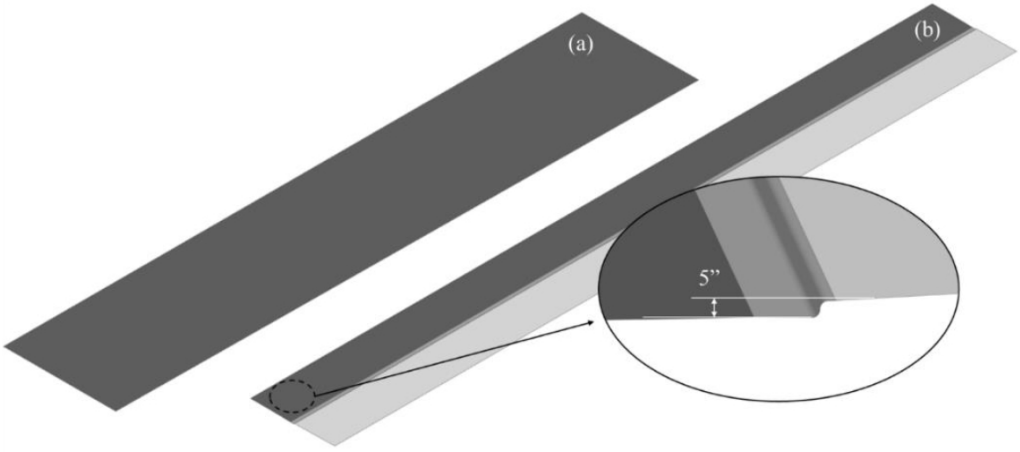

Figure 6. FE models of a flat road surface (**a**) and flat road surface with a curb (**b**).

2.6. Contact Modeling

In numerical simulations, various and appropriate contact algorithms were employed to properly capture the multifaceted interaction characteristics of vehicular impacts. The primary vehicle-to-mailbox interaction was modeled using *CONTACT_AUTOMATIC_SURFACE_TO_SURFACE, with static and dynamic friction coefficients of 0.4. A segment-based contact method (SOFT = 2) was applied with a scale factor (SOFSCL) of 0.1, effectively accommodating mesh size disparities between the vehicle and mailbox components. Additionally, maximum penetration checks (PENCHK = 0) ensured robust contact behavior, especially during large deformations.

The tire-to-road interface was represented using *CONTACT_AUTOMATIC_SURFACE_TO_SURFACE_ID. This contact incorporated static and dynamic friction coefficients of 0.5, alongside a viscous damping coefficient (VDC) of 20.0 to minimize numerical oscillations and maintain contact stability. Full-state outputs for this interaction were generated every 0.001 s to ensure high temporal resolution. Bolt connections were modeled using *CONTACT_AUTOMATIC_SINGLE_SURFACE, with static and dynamic friction coefficients of 0.2 and 0.1, and a damping coefficient (DC) of 0.001. These contact definitions included contact depth parameters (DEPTH = 5) and bucket sort frequencies (FRCFRQ = 1) to enhance numerical stability during impact simulations.

The self-contact behavior of the mailbox components was captured using *CONTACT_AUTOMATIC_SINGLE_SURFACE, with static and dynamic friction coefficients of 0.2 and 0.15, respectively. The segment-based method (SOFT = 2) was employed to model self-contact during extensive deformations and supported by a scale factor (SOFSCL) of 0.1. The *CONTACT_AUTOMATIC_NODES_TO_SURFACE_ID was defined for dummy-

to-seat and pelvis-to-seat interactions. These contacts incorporated damping parameters (DC = 0.001) and penetration limits to prevent numerical artifacts.

The contact configuration for the steering column adopted *CONSTRAINED_JOINT_SPHERICAL_ID, which defined spherical rotational constraints with a rotational proportional stiffness (RPS) of 0.1 and a damping coefficient of 1.0. Airbag deployment interactions were modeled using *CONTACT_AUTOMATIC_SURFACE_TO_SURFACE_ID, with static and dynamic friction coefficients of 0.5 and a viscous damping coefficient (VDC) of 40.0. The airbag-to-occupant interaction was further refined with penetration tolerance checks and detailed dynamic parameters, ensuring accurate simulation of airbag expansion and occupant engagement.

For other interactions such as the seatbelt-to-neck contact, *CONTACT_AUTOMATIC_SURFACE_TO_SURFACE was defined with static and dynamic friction coefficients of 0.2, along with detailed damping and sorting parameters to accurately model the restraint system. Across all contact definitions, bucket sort frequencies (FRCFRQ = 1) and element depth parameters (DEPTH = 5) were applied to ensure computational efficiency while maintaining physical realism throughout the simulations.

3. Simulation Setups

3.1. Vehicular Impact Conditions

In this study, the CMs were evaluated under MASH TL-1 impact conditions [30] that involved two test vehicles, a 1100C passenger car and a 2270P pickup truck, represented by the Toyota Yaris and Ford F250, respectively. In these impact scenarios, the impact speed was 50 km/h, and the impact angles were 0° and 25°. For the Toyota Yaris, with a total mass of 1170 kg including the occupant and interior components, the initial kinetic energy at 50 km/h impact velocity was 113 kJ. The Ford F250, having a substantially higher mass of 2700 kg, possessed an initial kinetic energy of 260 kJ at the same impact velocity. At a 0° impact angle, the vehicle crashed into the CMs from the side, with the centerline of the test vehicle aligned with that of the CMs, as defined in MASH. For the 25° impacts on the dual-unit CMs, MASH does not specify the initial impact location; hence, two impact points were chosen to determine the most critical crash scenario—the nearest corner and the midpoint, as illustrated in Figure 7. The impact angle was defined as the angle between the travel direction of the vehicle and the front face of the CMs.

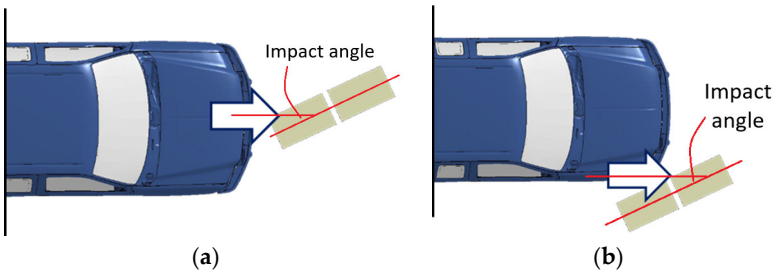

Figure 7. Two impact locations for crash simulations of dual-unit CMs. (**a**) At the nearest corner and (**b**) at the midpoint.

3.2. Simulation Matrix of Various Impact Scenarios

The simulations were divided into two groups based on CM configurations, single and dual units, each of which involved two CM models (Type I and Type IV) and two test vehicles (Toyota Yaris and Ford F250). For single-unit configurations, there were three impact conditions (S1 to S3) based on the road surface types (flat road with and without a curb) and impact angles (0° and 25°):

S1: CM on a flat road and impacted by the vehicles at 0°.

S2: CM on a flat road and impacted by the vehicles at 25°.

S3: CM placed 2.44 m (8 ft) behind a curb and impacted by the vehicles at 25°.

For dual-unit configurations, there were five impact conditions (D1 to D5) based on the road surface types (flat road with and without a curb), impact angles (0° and 25°), and initial impact locations (at the nearest corner and at the midpoint):

D1: CM on a flat road and impacted by the vehicles at 0°.

D2: CM on a flat road and impacted by the vehicles at the nearest corner at 25°.

D3: CM on a flat road and impacted by the vehicles at the midpoint at 25°.

D4: CM placed 2.44 m (8 ft) behind a curb and impacted by the vehicles at the nearest corner at 25°.

D5: CM placed 2.44 m (8 ft) behind a curb and impacted by the vehicles at the midpoint at 25°.

There were twelve simulations for single-unit configurations (two types of CM, two vehicles, and three impact conditions) and twenty simulations for dual-unit configurations, resulting in a total of thirty-two simulations for this study. The impact speed was 50 km/h for all simulation cases. Figure 8 illustrates the eight impact conditions using the 2010 Toyota Yaris and the Type I CMs. Note that in the last image of Figure 8, the single-unit CM was used to illustrate the CM placement behind a curb. For impact conditions D4 and D5, dual-unit CMs were used in place of the single-unit CM. The simulation matrix shown in Table 1 was applied to both the Type I and Type IV CMs. The simulations were carried out using the massively parallel processing (MPP) version of LS-DYNA 9.0.1, executed on a high-performance computing cluster with 16 processors and 125 GB of allocated memory. Each impact scenario was analyzed over a duration of 0.5 s, employing a time scale factor (TSSFAC) of 0.9 and a minimum time step threshold of 5.5550×10^{-7} s. Selective mass scaling was enabled so that nonphysical mass was applied exclusively to elements with time steps below the specified threshold. This ensured numerical stability while maintaining the physical accuracy of the simulation results.

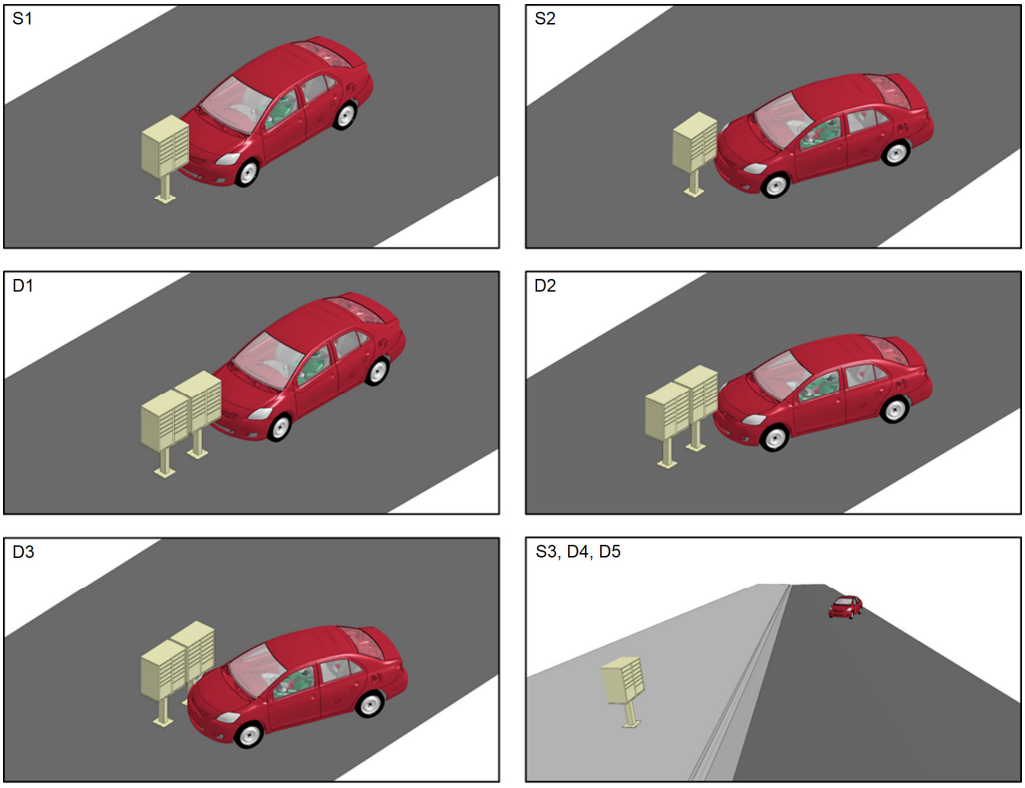

Figure 8. Illustration of impact conditions S1–S3 and D1–D5 using a 2010 Toyota Yaris.

Table 1. Simulation matrix for Type I or Type IV CMs of this study.

Impact Condition S: Single; D: Double	Road Surface	Impact Angle	Impact Point	Impact Vehicle
S1	No curb	0°	Side	Toyota Yaris
				Ford F250
S2	No curb	25°	Corner	Toyota Yaris
				Ford F250
S3	With curb	25°	Corner	Toyota Yaris
				Ford F250
D1	No curb	0°	Side	Toyota Yaris
				Ford F250
D2	No curb	25°	Corner	Toyota Yaris
				Ford F250
D3	No curb	25°	Midpoint	Toyota Yaris
				Ford F250
D4	With curb	25°	Corner	Toyota Yaris
				Ford F250
D5	With curb	25°	Midpoint	Toyota Yaris
				Ford F250

The simulation employed two distinct temporal resolutions for data acquisition: time history data were captured at an interval of 8.0×10^{-5} s, while full-state data for visualization purposes was output every 0.001 s. The impact of selective mass scaling was closely monitored using GLSTAT and MATSUM databases, which provided insights into the distribution and magnitude of added mass during the simulation.

3.3. Occupant Risk Assessment Criteria

Occupant injury risk was evaluated using both vehicular and dummy responses. For vehicular responses, the following MASH evaluation criteria were used:

- Criterion *D*: no intrusion into the occupant compartment from detached fragments or debris;
- Criterion *F*: the maximum roll and pitch angles of the vehicle do not exceed 75°;
- Criterion *G*: the longitudinal or lateral occupant impact velocities (OIVs) do not exceed 12.2 m/s (40 ft/s), with preferred values under 9.1 m/s (30 ft/s);
- Criterion *I*: the longitudinal or lateral occupant ride-down accelerations (ORAs) do not exceed 20.49 G, with preferred values under 15.0 G, where G is the gravitational acceleration.

It should be noted that both OIVs and ORAs were determined using vehicular responses at the instant when a "hypothetical occupant" collided with the vehicle compartment. These indices were determined in both the longitudinal and lateral directions. The ORA value is defined as the highest value of the vehicle accelerations averaged over a 10-millisecond interval following the hypothetical occupant's collision with the vehicle's interior. The calculations of OIV and ORA were thoroughly discussed in the study by Li et al. [32].

The time histories of dummy head accelerations were used to determine the likelihood of skull fracture, using the head injury criteria (HIC), calculated as follows:

$$HIC = Max\left\{(t_2 - t_1)\left[\frac{\int_{t_1}^{t_2} a(t)dt}{t_2 - t_1}\right]^{2.5}\right\} \quad (1)$$

where $a(t)$ denotes the resultant accelerations (in G), and t_1 and t_2 are the starting and ending time that define the time interval of $(t_2 - t_1)$. For the commonly used HIC_{15}, $(t_2 - t_1)$ shall not exceed 15 ms. The likelihood of having a skull fracture injury was determined by the HIC value as defined by Hertz [37]:

$$p(HIC) = \frac{1}{\sqrt{2\pi}}\int_{-\infty}^{\frac{\ln(HIC) - 6.96352}{0.84664}} e^{\frac{-t^2}{2}}\, dt \quad (2)$$

For adults, the HIC_{15} threshold value is 700, corresponding to a 31% chance of receiving a skull fracture injury.

4. Results and Discussions

The vehicular responses and the dummy head accelerations were obtained for the simulations, and the collision courses and vehicle trajectories are presented and discussed, providing a detailed insight into the impact dynamics.

4.1. Single-Unit CMs (Type I and Type IV)

The single-unit Type I and Type IV CMs were tested using the two test vehicles under three impact conditions (S1–S3) as described in Section 3.2. Tables 2 and 3 summarize the vehicular responses (i.e., OIVs, ORAs, maximum roll and pitch angles) and occupant safety factors (i.e., HIC_{15} and probability of fracture) for Type I and Type IV CMs, respectively. The following subsections present results of single-unit Type I and Type IV CMs for each of the three impact conditions.

Table 2. Occupant safety factors for the single-unit Type I CM.

Impact Condition	Test Vehicle	OIV (m/s)		ORA (G)		Vehicular Angular Motion		Occupant Injury	
		OIVx	OIVy	ORAx	ORAy	Max. θ_{roll}	Max. θ_{pitch}	HIC_{15}	$p(HIC_{15})$
S1	Yaris	3.45	0.02	3.53	4.06	0.57°	0.60°	2.90	0%
	F250	1.45	0.20	1.88	0.90	1.03°	0.72°	1.38	0%
S2	Yaris	3.45	0.08	0.81	1.03	0.68°	1.47°	3.72	0%
	F250	1.60	0.17	1.02	0.96	2.87°	0.92°	0.73	0%
S3	Yaris	1.69	0.47	5.09	3.11	4.24°	1.81°	0.91	0%
	F250	1.09	0.27	4.03	3.00	5.96°	1.73°	8.98	0%

Table 3. Occupant safety factors for the single-unit Type IV CM.

Impact Condition	Test Vehicle	OIV (m/s)		ORA (G)		Vehicular Angular Motion		Occupant Injury	
		OIVx	OIVy	ORAx	ORAy	Max. θ_{roll}	Max. θ_{pitch}	HIC_{15}	$p(HIC_{15})$
S1	Yaris	3.52	0.08	1.05	1.84	0.57°	1.05°	1.52	0%
	F250	1.63	0.04	2.46	0.69	1.16°	0.52°	1.44	0%
S2	Yaris	3.69	0.24	1.09	1.41	0.51°	0.75°	2.99	0%
	F250	1.83	0.26	0.93	1.00	0.71°	0.64°	0.66	0%
S3	Yaris	1.87	0.52	5.52	3.78	7.74°	7.34°	3.09	0%
	F250	1.09	0.30	4.10	3.16	6.13°	2.52°	1.53	0%

4.1.1. Impact Condition S1

The vehicle trajectories during the vehicular impact scenarios were captured at three critical time intervals, 0, 60, and 120 ms, to demonstrate the progression of the vehicle's

interaction with the single-unit Type I CM. Figure 9 shows these three key stages of vehicle motion and CM displacement during the crash event.

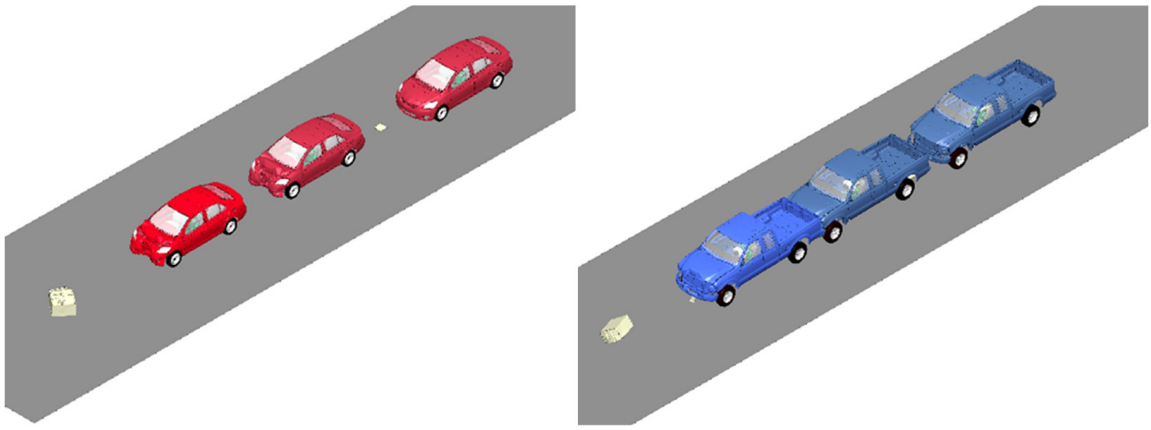

(**a**) (**b**)

Figure 9. Vehicle trajectories during impacts on the single-unit Type I CM at 0° on a flat road at 0, 60, and 120 ms. (**a**) Toyota Yaris (1100C) and (**b**) Ford F250 (2270P).

At 0 ms, the vehicles were at their initial positions that were aligned just before contacting the CM. At 60 ms, the pedestal of the CM impacted by Toyota Yaris was detached and pushed forward, with the upper unit tilted slightly but remaining connected to the pedestal. For the heavier Ford F250, the pedestal was pushed under the chassis, showing a more aggressive interaction. At 120 ms, the CM upper unit caused severe damage to Toyota Yaris and was knocked off the pedestal and displaced forward. The Ford F250 experienced minor damage by the upper unit of the CM. In both cases, the upper CM unit remained structurally intact, with minor slot door deformations. The front body of the Yaris was severely damaged, resulting in a crumpled hood and bent bumper, as seen in Figure 10a. When impacted by the Ford F250, the pedestal was pushed underneath the chassis, leading to a minor dent on the vehicle's front hood as shown in Figure 10b. For both vehicles, the OIV and ORA values, as well as the maximum roll and pitch angles, were far below the MASH preferred and limit values.

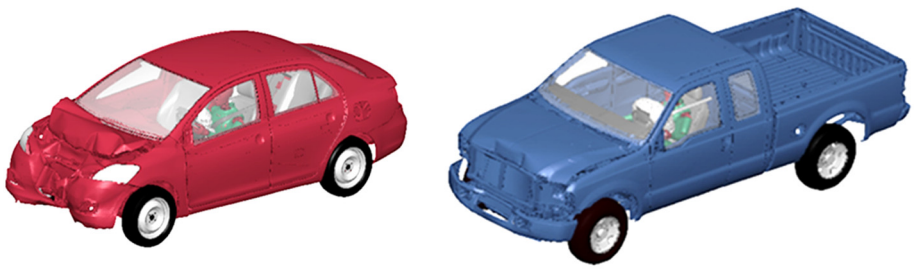

(**a**) (**b**)

Figure 10. Vehicle damage after impacting the single-unit Type I CM at 0° on a flat road. (**a**) Toyota Yaris (1100C) and (**b**) Ford F250 (2270P).

Figure 11 shows the time histories of dummy head accelerations during the two impacts on the Type I CM, from which the HIC_{15} values were calculated and shown to be well under the MASH limit value, 700, resulting in a 0% chance of having a skull fracture. Throughout the entire crash event, the dummy's head was not in contact with the deployed airbags, indicating no apparent risk of injury to the occupant in both impact scenarios.

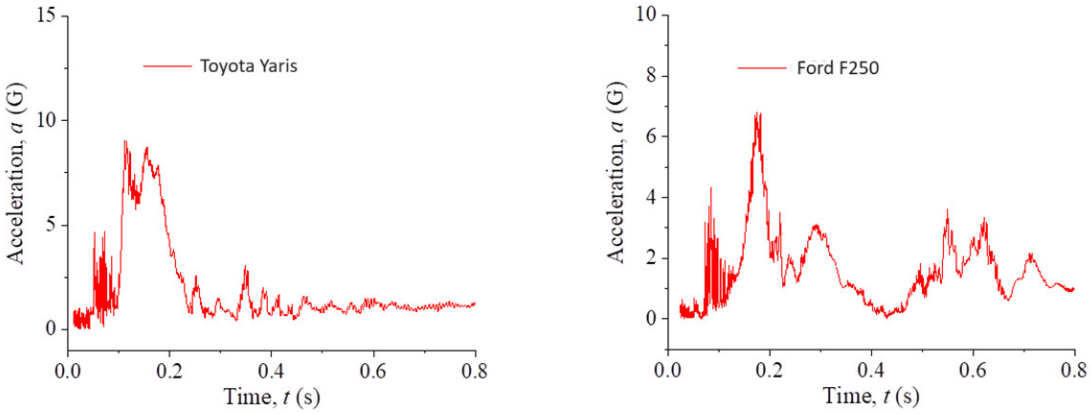

Figure 11. Head resultant accelerations from the 0° impact on the single-unit Type I CM on a flat road.

Under impact condition S1, the simulation results of the Type IV CM showed similar vehicular responses to, and comparable safety factors as, the Type I CM (see Tables 2 and 3).

4.1.2. Impact Condition S2

Figure 12 shows the sequence of dynamic interactions between the Toyota Yaris and the Type IV CM in the 25° impact on a flat road surface. The snapshots, taken at 20, 60, and 100 ms, depict the progressive deformation and displacement of both the CM and the vehicle.

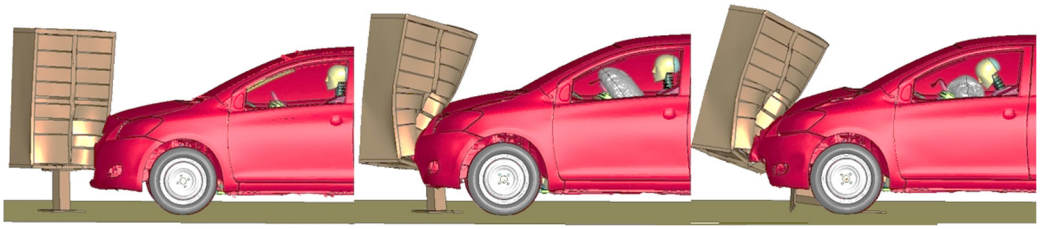

Figure 12. Sequential snapshots of the Toyota Yaris (1100 kg) impacting the Type IV cluster mailbox (CM) at a 25° angle on a flat road surface at 20, 60, and 100 ms.

At 20 ms, the vehicle deformed the upper unit of the CM, leading to the initial tilting of the pedestal. At this stage, the deformation was localized around the point of contact on the CM and the vehicle. The hood of the Toyota Yaris showed slight crumpling, absorbing some of the collision energy. Inside the vehicle, the dummy was restrained by the seatbelt system and had no significant forward movement. At 60 ms, the CM was significantly displaced, with visible deformation on its upper body, especially near the impact location. The vehicle's hood continued to crumble and absorbed the impact energy. The dummy remained upright, with no excessive forward displacement. The airbag, although deployed, did not contact the dummy that was restrained by the seatbelt system.

By 100 ms, the pedestal was fully dislodged from the base, although it remained attached to the upper CM body. The upper unit showed substantial deformation but retained its structural integrity. The vehicle exhibited significant deformation on the front end, with severe hood and bumper crumpling. The dummy head contacted the deployed airbag, but the HIC_{15} value was well below the critical threshold, indicating no potential injury risks. For Ford F250 under impact condition S2, the pedestal was sheared off from the CM body and pushed beneath the vehicle chassis due to the high impact force. The deformation of the Ford F250's front end was less severe than that of the Toyota Yaris due to the former's elevated bumper and robust construction. The dummy safety factors,

including HIC_{15} value, were also well within safe limits and thus indicated no risk of occupant injuries.

4.1.3. Impact Condition S3

When placed behind a curb, the single-unit Type I CM had reduced impact severity compared to the "no curb" test cases. In both cases, the pedestal remained attached to the upper unit of the CM but detached from the ground at the base. The maximum roll and pitch angles and the ORA values in the longitudinal direction were all increased due to impacting the curb. Figure 13 compares the post-crash deformation of the two vehicles after impacting the Type I CM at a 25° angle under two different road conditions: without a curb (upper row) and with a curb (lower row). For the Toyota Yaris, the presence of the curb slightly reduced the severity of damage, particularly on the front-end deformation, due to the altered impact dynamics by the curb. By contrast, Ford F250 showed no significant difference in damage between the two conditions, suggesting that the larger vehicle's structure and impact characteristics were less affected by the curb.

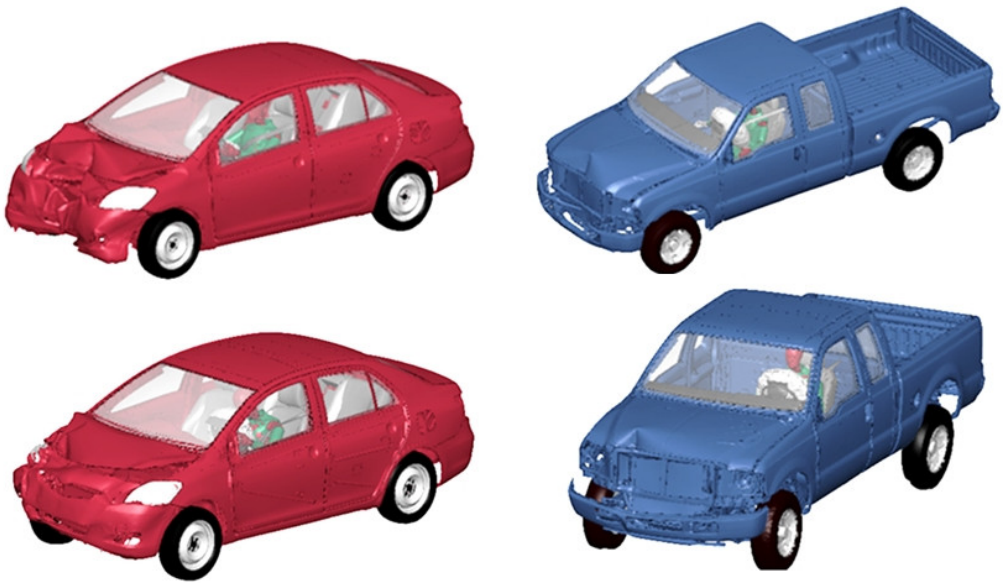

Figure 13. Post-crash deformation of the Toyota Yaris (**left**) and Ford F250 (**right**) after impacting the Type I CM at 25° under two road conditions: without a curb (**top**) and with a curb (**bottom**).

The peak value of the dummy head resultant acceleration occurred at 1.3 s in the case of Ford F250 was regarded as a numerical noise from the dummy model since the dummy head had no contact with the deployed airbag. The values of OIV, ORA, and HIC_{15} were all below the MASH limiting values, indicating a low risk of occupant injury. For the single-unit Type IV CM installed behind a curb, the vehicular responses and safety factors were like those for the Type I CM, except for the case with the Toyota Yaris in which the dummy's head moved and struck the deployed airbag during collision and resulted in an increased HIC_{15} value. For both single-unit Type I and Type IV CMs, the simulation results and safety factors indicated no or extremely low occupant injury risk under all three impact conditions.

4.2. Dual-Unit CMs (Type I and Type IV)

The dual-unit Type I and Type IV CMs were tested using the two test vehicles under five impact conditions (D1–D5) as described in Section 3.2. Tables 4 and 5 summarize the vehicular responses (i.e., OIVs, ORAs, maximum roll and pitch angles) and occupant safety factors (i.e., HIC_{15} and probability of fracture) for the Type I and Type IV CMs, respectively.

Table 4. Occupant safety factors for the dual-unit Type I CM.

Impact Condition	Test Vehicle	OIV (m/s)		ORA (G)		Vehicular Angular Motion		Occupant Injury	
		OIVx	OIVy	ORAx	ORAy	Max. θ_{roll}	Max. θ_{pitch}	HIC_{15}	$p(HIC_{15})$
D1	Yaris	5.14	0.07	1.70	4.17	0.69°	1.91°	9.02	0%
	F250	2.20	0.22	1.51	0.85	1.19°	0.81°	1.08	0%
D2	Yaris	5.11	0.37	3.04	1.82	1.57°	0.58°	7.64	0%
	F250	2.64	0.13	1.63	1.13	1.27°	0.95°	1.20	0%
D3	Yaris	3.53	0.10	0.99	1.05	0.46°	0.85°	2.65	0%
	F250	1.98	0.42	1.38	1.68	3.55°	0.80°	5.16	0%
D4	Yaris	1.86	0.43	6.56	2.82	4.35°	5.18°	2.37	0%
	F250	2.31	0.49	3.08	1.75	6.36°	1.44°	1.36	0%
D5	Yaris	1.65	0.86	2.59	2.77	4.35°	1.82°	0.30	0%
	F250	1.11	0.29	5.03	3.27	6.36°	2.19°	2.55	0%

Table 5. Occupant safety factors for the dual-unit Type IV CM.

Impact Condition	Test Vehicle	OIV (m/s)		ORA (G)		Vehicular Angular Motion		Occupant Injury	
		OIVx	OIVy	ORAx	ORAy	Max. θ_{roll}	Max. θ_{pitch}	HIC_{15}	$p(HIC_{15})$
D1	Yaris	6.36	0.18	3.59	3.22	0.89°	3.13°	9.70	0%
	F250	3.12	0.02	2.28	2.04	1.01°	0.73°	1.95	0%
D2	Yaris	5.99	0.45	6.09	4.96	3.24°	2.38°	15.89	0%
	F250	2.81	0.19	4.10	3.54	1.22°	0.57°	1.27	0%
D3	Yaris	3.75	0.63	1.39	2.44	2.87°	0.89°	4.63	0%
	F250	1.74	0.46	1.44	0.96	1.17°	0.66°	2.89	0%
D4	Yaris	1.81	0.85	7.74	5.20	6.19°	7.57°	7.88	0%
	F250	2.67	0.48	3.24	3.73	6.31°	2.53°	2.51	0%
D5	Yaris	1.68	0.86	4.41	2.28	4.41°	1.80°	2.68	0%
	F250	2.12	1.18	3.80	3.21	6.08°	2.92°	5.04	0%

4.2.1. Impact Condition D1

Under this impact condition, the test vehicles impacted the dual-unit Type I CM at a 0° angle. The vehicle trajectories and damage are shown in Figures 14 and 15, respectively. In both cases, the pedestals did not break off from the upper units upon initial impacts due to support from the other units. As the test vehicle ran over the pedestals, the upper units were separated and pushed away from the pedestals. The dual-unit CM caused larger deformations on test vehicles than the single-unit CM; this could be seen from the warped and wrinkled front hood of the Toyota Yaris and a large flat dent with a partially popped-up front hood on the Ford F250. The occupant safety factors shown in Table 4 were generally larger than those of the single-unit CM.

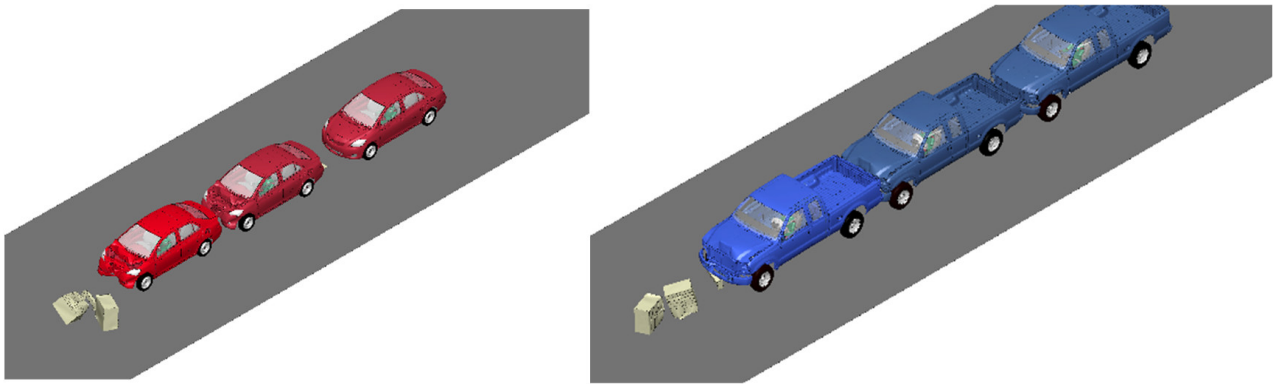

(**a**) (**b**)

Figure 14. Vehicle trajectory during the 0° impact on the dual-unit Type I CM. (**a**) Toyota Yaris (1100C) and (**b**) Ford F250 (2270P).

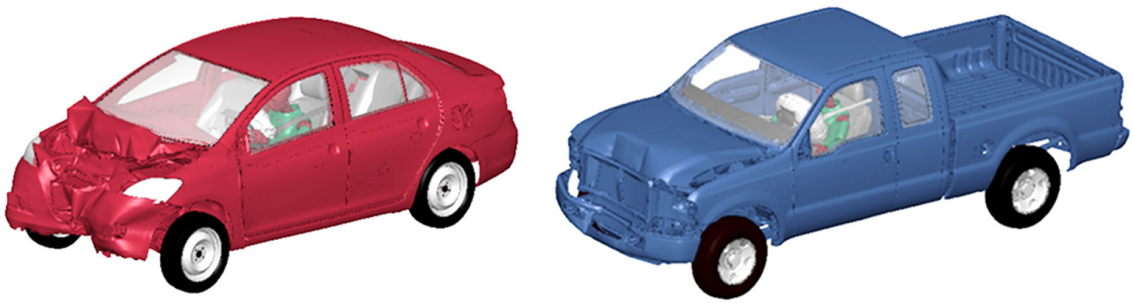

(**a**) (**b**)

Figure 15. Vehicle damage after impacting the dual-unit Type I CM at 0° on a flat road. (**a**) Toyota Yaris (1100C) and (**b**) Ford F250 (2270P).

The maximum resultant head acceleration from impact by the Toyota Yaris was approximately 14 G, much higher than that by the Ford F250 (see Figure 16). Nonetheless, all safety factors in Table 4 were within the safety limits and indicated no occupant injury risk for the dual-unit Type I CM.

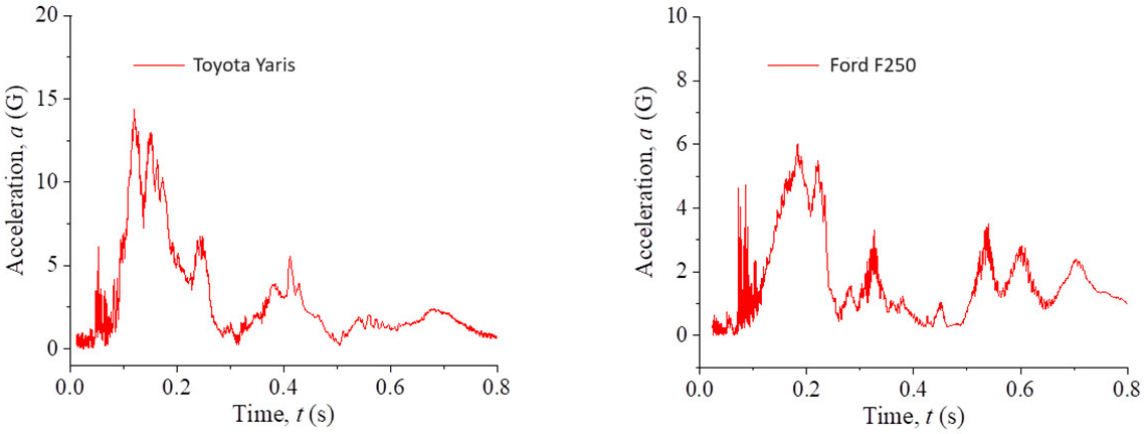

Figure 16. Head resultant accelerations from the 0° impact on the dual-unit Type I CM.

The dual-unit Type IV CM, due to its greater mass, caused larger damage to the front area of the test vehicles than that by the Type I CM. The upper units immediately separated from the pedestals upon impact by the test vehicles, with the first-hit unit having more damage than the second one. Although the longitudinal ORA and OIV values were larger than those for the Type I CM, they were well below the MASH limit values, with a similar HIC_{15} value. Based on the safety factors in Table 5, no potential occupant injury was indicated for the dual-unit Type IV CM.

4.2.2. Impact Conditions D2 and D3

Figure 17 shows the progressive structural deformation and damage of the dual-unit Type IV CM under impact of Toyota Yaris at a 25-degree angle at the nearest corner.

The initial phase of the impact generated high stress concentrations at the base of the pedestal columns and localized bending at the lower part of the CM upper unit. As the deformation progressed, the support columns underwent significant plastic deformation and failed at the base. This compromised the structural stability of the system and triggered a cascade of failures in the upper units. The main body of the CM experienced asymmetric crushing and folding, particularly in the regions directly under impact. Vertical panels displayed outward deformation due to axial compression, while horizontal panels exhibited bending and folding, forming localized plastic hinges.

The upper units of the CM exhibited progressive panel buckling and structural separation. The interaction between the vehicle and the CM caused a redistribution of forces, resulting in further deformation of the attachment points at the base and eventually rendering the unit detached from its foundation. Under impact by the Ford F250, the upper bodies of both units separated from the pedestals, and the vehicle ran over the second unit's pedestal while pushing the upper body forward, causing a large V-shaped dent on the hood of the Ford F250.

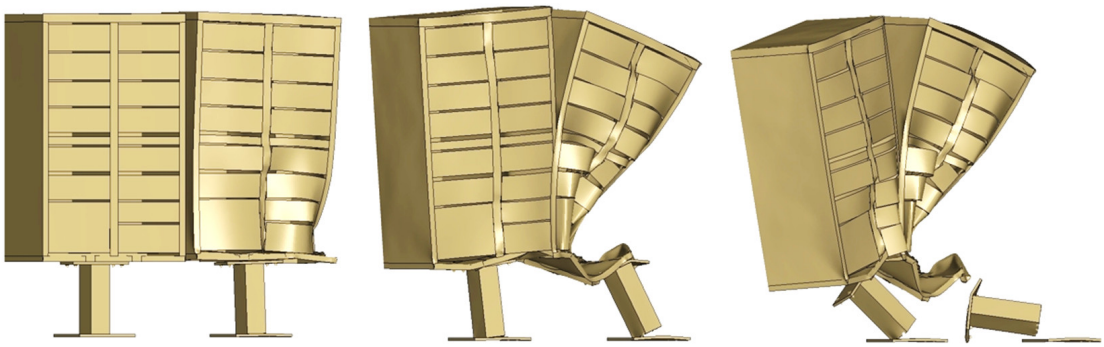

Figure 17. Sequential deformation of the dual-unit Type IV CM impacted by Toyota Yaris at 25° and at the nearest corner on a flat road. Time steps shown are 20, 80, and 120 ms.

The kinetic energy dissipation of Toyota Yaris impacting the dual-unit Type IV CM at 25° is shown in Figure 18. The initial kinetic energy of the vehicle was approximately 113 kJ, which gradually dissipated through progressive CM and vehicle deformations and friction losses during the collision event. The residual kinetic energy remained on the CM and the vehicle as they continued moving forward. The steep decline in kinetic energy during the initial stage of the collision indicated a rapid energy transfer into structural deformation and the initiation of failure in the impacted CM. Towards the end of the simulation, the vehicle's residual velocity was approximately 18.11 km/h, accounting for a portion of the remaining kinetic energy.

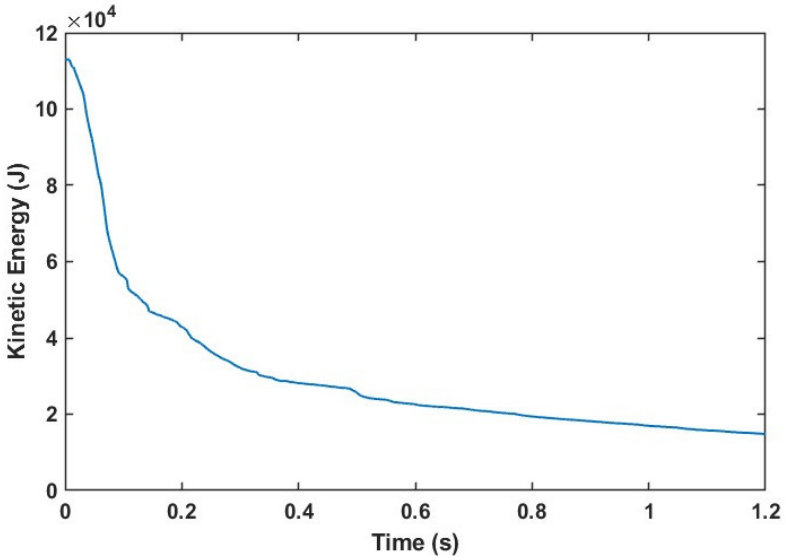

Figure 18. Kinetic energy dissipation of the Toyota Yaris during impact with the dual-unit Type IV CM at a 25° angle and at the nearest corner.

Under impact condition D3, the damage on both test vehicles was minor compared to that under impact condition D2. Under impact by the Toyota Yaris, the first unit

remained at its original location, and the second unit was separated from the ground and pushed forward. The impact left minor damage on the hood and popped it open on the passenger side. Under impact by the Ford F250, the CM responded similarly to those by the Toyota Yaris. The occupant safety factors in Table 4 showed that the impacts at midpoint were less severe than impacts at the nearest corner; the longitudinal OIV and ORA were approximately 30% and 70% lower, respectively, than those from impacts at the nearest corner.

For the dual-unit Type I CM under impact conditions D2 and D3, vehicular trajectories and damage patterns, as well as mailbox responses, were like those from the Type IV CM. Vehicular damage in the impacts at midpoint were smaller than those from impacts at the nearest corner. Vehicular damage was generally larger by the Type IV CM due to its larger mass than by the Type I CM. The simulation results showed no risk of any mailbox components intruding into the occupant compartment, and the safety factors in Table 5 indicated no significant risk of occupant injury.

4.2.3. Impact Conditions D4 and D5

Under impact conditions D4 and D5, the dual-unit Type I and Type IV CMs were placed eight feet from the curb face. The test vehicles "climbed up" the curb and impacted the CMs at a 25° angle at two locations: at the nearest corner and at the midpoint of the dual-unit CMs.

Figure 19 shows the vehicle trajectories of the two vehicles impacting the Type I CM at the nearest corner (impact condition D4). When impacted by the Toyota Yaris, the two units were pushed forward together with the pedestals attached to the upper units. Under impact by the Ford F250, the first unit was immediately separated from the ground, and its upper body became wedged between the vehicle and the second unit and eventually separated from the pedestal. The damage on both vehicles, as shown in Figure 20, was less severe than that on the respective vehicles under impact condition D2 (without curb). This observation was consistent with observation on the single-unit Type I CM, where the curb caused less severe damage to the striking vehicles. For both impacts, there was no potential risk of the CM components penetrating the windshield and entering the occupant compartment.

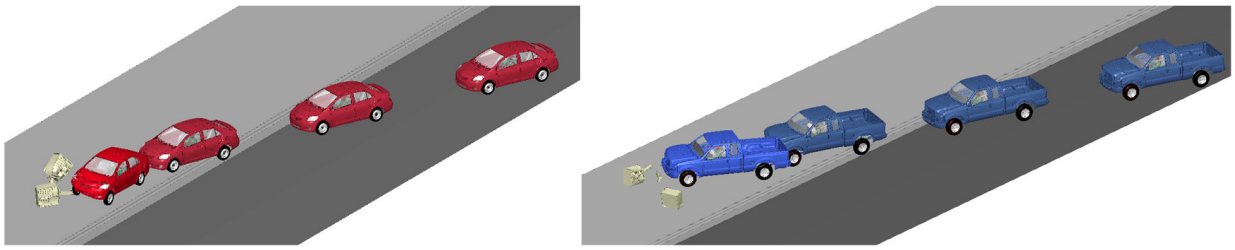

(**a**) (**b**)

Figure 19. Vehicle trajectory during impact at the nearest corner of dual-unit Type I CM behind a curb (D4). (**a**) Toyota Yaris (1100C) and (**b**) Ford F250 (2270P).

Figure 21 shows the trajectories of the test vehicles impacting at the midpoint of the dual-unit Type I CM behind a curb (impact condition D5). The Yaris only grazed the first unit before pushing the second unit until it bent backward. Both pedestals did not detach from the ground, and the Yaris was left with minor deformations, as shown in Figure 22a, and the face of the dummy did not touch the deployed airbag. For the Ford F250, the first unit remained at its original location, and the second unit was pushed forward along with the initial impact direction; this left a localized deformation on the front right corner of

the Ford F250, as seen in Figure 22b. There was no potential risk of the CM components penetrating the windshield and entering the occupant compartment.

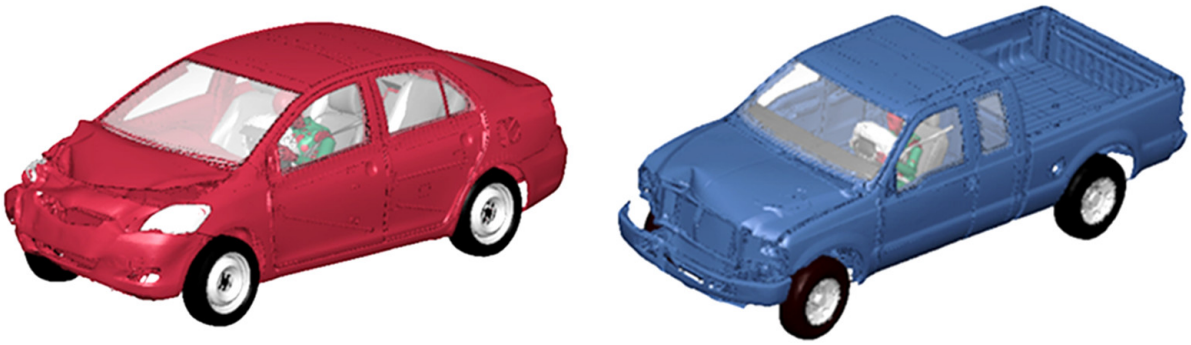

(**a**) (**b**)

Figure 20. Vehicle damage after impacting at the nearest corner of dual-unit Type I CM behind a curb (D4). (**a**) Toyota Yaris (1100C) and (**b**) Ford F250 (2270P).

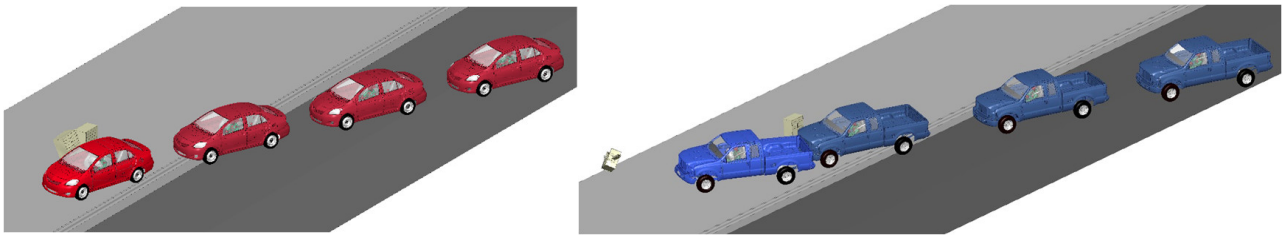

(**a**) (**b**)

Figure 21. Vehicle trajectory during impact at midpoint of dual-unit Type I CM behind a curb (D5). (**a**) Toyota Yaris (1100C) and (**b**) Ford F250 (2270P).

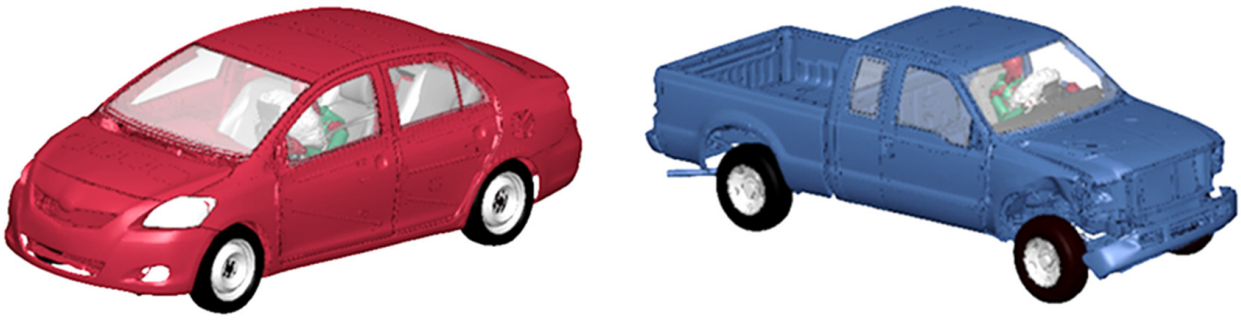

(**a**) (**b**)

Figure 22. Vehicle damage after impacting at midpoint of dual-unit Type I CM behind a curb (D5). (**a**) Toyota Yaris (1100C) and (**b**) Ford F250 (2270P).

The time histories of dummy head accelerations are shown in Figures 23 and 24 for impact locations at the nearest corner and at the midpoint, respectively, of the dual-unit Type I CM. The occupant safety factors under impact conditions D4 and D5 were then calculated, as summarized in Table 4; they were far below the safety limits required by MASH and therefore indicated no potential occupant injuries.

For the dual-unit Type IV CM, the impacts at the midpoint were generally less severe than those at the nearest corner, reflecting the pattern observed on the dual-unit Type I CM. No CM components were found to intrude into the vehicles' compartments, and all the safety factors were well below the MASH limit values, indicating no potential risk of occupant injury.

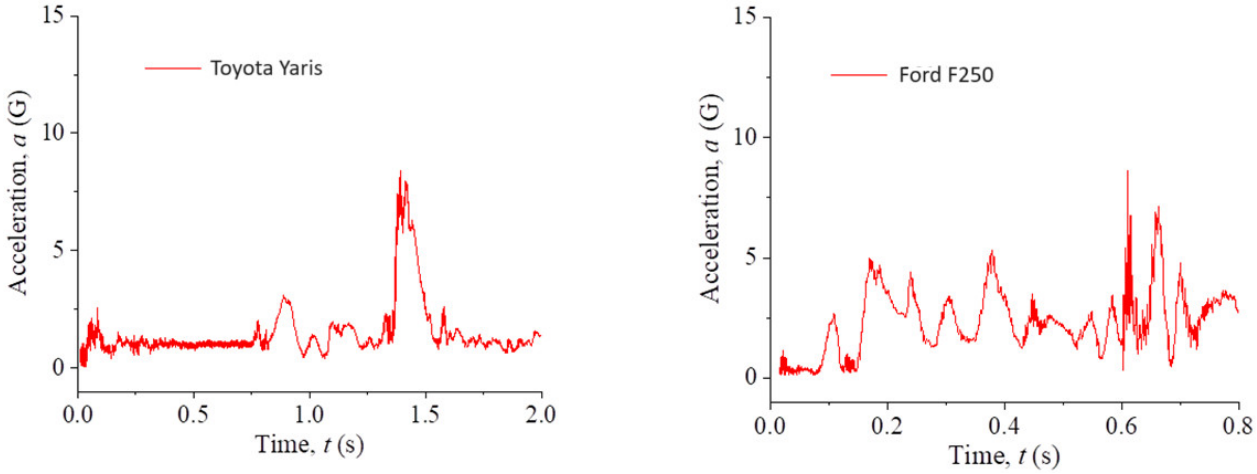

Figure 23. Head resultant accelerations from the 25° impacts at the nearest corner of dual-unit Type I CM behind a curb (D4).

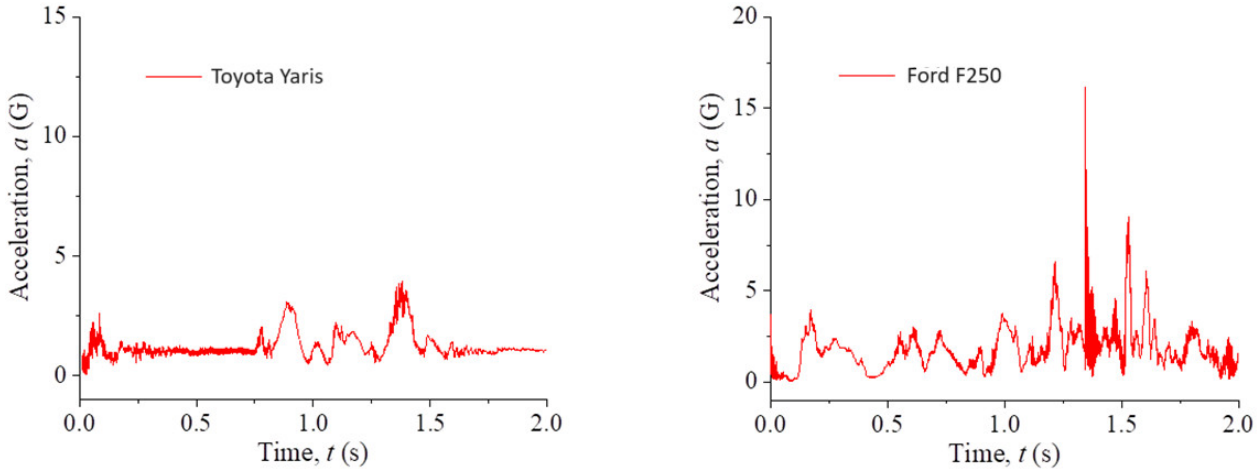

Figure 24. Head resultant accelerations from the 25° impacts at midpoint of dual-unit Type I CM behind a curb (D5).

5. Concluding Remarks

In this study, two types of cluster mailboxes (CMs) were tested and assessed in terms of their safety for road users using nonlinear finite element analysis. In the analysis, the course of the vehicle collision with the CMs, damage to the CMs and vehicles, and the potential injuries of the occupant were thoroughly evaluated. For each of the two types of CMs, i.e., Type I and Type IV, a series of simulations were conducted with the following variables considered:

- Two test vehicles: 2010 Toyota Yaris (model 1100C) and 2006 Ford F250 (model 2270P);
- Two CM configurations: single- and dual-unit CMs;
- Two road surface types: a flat road with and without a curb;
- Two impact angles: 0° and 25°;
- Two impact locations for the 25° impacts on the dual-unit CMs: at the nearest corner and at the midpoint.

This resulted in a total of 32 crash cases, 16 for each of the two Types of CMs. All the tests were conducted with the same initial impact speed of 50 km/h. In all crash simulations, the vehicle models included seat belts, airbags, and a Hybrid III 50th percentile male test dummy. The dummy enabled one to analyze the occupant responses and to record

the time histories of head accelerations. The data were used to determine the following impact severity indices: OIV, ORA, and HIC. The simulations yielded valuable insights into occupant risks when CMs were involved in vehicular crashes. The most important findings from the research are summarized below.

In scenarios involving single-unit CMs, the primary mode of failure was the detachment of the upper unit from its pedestal. As a result of the impact, the upper unit sustained significant damage to the frontal face, while the vehicle had minimal damage that was localized to the hood of the vehicle. It should be highlighted that the CM components did not intrude into the occupant compartment. The roll and pitch angles of the vehicles, the OIV and ORA values, and the HIC_{15} values were all under the thresholds defined by MASH, indicating a negligible risk of occupant injury. To conclude, vehicular collisions with the single-unit Type I and Type IV CMs posed no risk or a marginal risk of injury to occupants.

For dual-unit CMs, the primary failure mechanism was the separation of upper bodies from the pedestals, same as the failure of the single-unit CMs. When impacted at the midpoint of the dual-unit CMs at a 25° impact angle, the first-hit unit remained almost intact in most cases, and the failure of the second unit was comparable to what was seen in the crashes with single-unit CMs. In crashes at the nearest corner of the dual-unit CMs, more severe damage to the test vehicles was observed than that in the single-unit cases. Despite the greater mass of the dual-unit CMs, no intrusion was observed from the mailbox components into the occupant compartment. The roll and pitch angles, OIVs, ORAs, and HIC_{15} values were all below the allowable limits specified by MASH. Consequently, no occupant injury risk was identified in the crash cases involving dual-unit Type I and Type IV CMs.

While valuable insights were gained from this study, additional investigations, e.g., using a 50th percentile female dummy or child dummies, would provide important data on how their responses might differ from those of male dummies, and on the risk profile in relation to the occupant's body mass. This study could also be expanded by including other vehicle models, particularly those that are lower to the ground or have different hood profiles, e.g., a USPS delivery truck, to determine if there are significant deviations in the safety evaluation results. It should be noted that the research findings were based on MASH TL-1 conditions and thus valid only for impact speeds up to 50 km/h. Additionally, the CMs were evaluated using numerical simulations, and experimental tests are needed to validate the research findings.

Author Contributions: Conceptualization, H.F.; Methodology, E.P., Q.W. and H.F.; Software, E.P., L.P. and D.B.; Validation, E.P., L.P., D.B. and Q.W.; Formal analysis, E.P. and H.F.; Investigation, E.P. and H.F.; Resources, H.F.; Data curation, E.P., C.J. and H.F.; Writing—original draft, E.P. and H.F.; Writing—review and editing, E.P., L.P., D.B., Q.W., C.J. and H.F.; Visualization, E.P. and C.J.; Supervision, H.F.; Project administration, H.F.; Funding acquisition, H.F. All authors have read and agreed to the published version of the manuscript.

Funding: The authors acknowledge the support of the North Carolina Department of Transportation (NCDOT) under Project No. NCDOT RP 2018-24, "Risk Assessment of Roadside Utility Structures under Vehicular Impacts".

Institutional Review Board Statement: Not applicable.

Informed Consent Statement: All authors approved the manuscript and agree with its submission to *Computation*.

Data Availability Statement: Data are available from the corresponding author upon request.

Conflicts of Interest: The authors declare no conflicts of interest.

References

1. AASHTO. *Manual for Assessing Safety Hardware (MASH)*, 2nd ed.; American Association of State Highway Transportation Officials: Washington, DC, USA, 2016.
2. Ross, H.E.; Walker, K.C. *Crash Tests of Rural Mailbox Installations*; Report No. 3254-6; Texas Transportation Institute, Texas A & M University: College Station, TX, USA, 1979.
3. Hall, P.R.; Ross, H.E. *Test and Evaluation of Rural Mailbox Supports*; Report No. 370-1F; Texas Transportation Institute, Texas A & M University: College Station, TX, USA, 1983.
4. Campise, W.L.; Ross, H.E. *Test and Evaluation of Neighborhood Mailbox*; Report No. FHWA/TX-84; Texas Transportation Institute, Texas A & M University: College Station, TX, USA, 1984.
5. Faller, R.K.; Magdaleno, J.A.; Warlick, B.A.; Wendling, W.H.; Post, E.R. Full-Scale Vehicle Crash Tests on Nebraska Rural Mailbox Designs. *Transp. Res. Rec.* **1987**, *1198*, 31–44.
6. Ross, H.E.; Bullard, L.; Alberson, D. *Mailbox Bracket Crash Test*; Report No. TX-94/1945-2F; Texas Transportation Institute, Texas A & M University: College Station, TX, USA, 1993.
7. Atahan, A.O. Development of a Heavy Containment Level Bridge Rail for Istanbul. *Lat. Am. J. Solids Struct.* **2018**, *15*, e81. [CrossRef]
8. Gutowski, M.; Palta, E.; Fang, H. Crash Analysis and Evaluation of Vehicular Impacts on W-beam Guardrails Placed Behind Curbs Using Finite Element Simulations. *Adv. Eng. Softw.* **2017**, *114*, 85–97. [CrossRef]
9. Gutowski, M.; Palta, E.; Fang, H. Crash Analysis and Evaluation of Vehicular Impacts on W-beam Guardrails Placed on Sloped Medians Using Finite Element Simulations. *Adv. Eng. Softw.* **2017**, *112*, 88–100. [CrossRef]
10. Hou, S.; Tan, W.; Zheng, Y.; Han, X.; Li, Q. Optimization Design of Corrugated Beam Guardrail Based on RBF-MQ Surrogate Model and Collision Safety Consideration. *Adv. Eng. Softw.* **2014**, *78*, 28–40. [CrossRef]
11. Yin, H.; Xiao, Y.; Wen, G.; Fang, H. Design Optimization of a New W-Beam Guardrail for Enhanced Highway Safety Performance. *Adv. Eng. Softw.* **2017**, *112*, 154–164. [CrossRef]
12. Ozcanan, S.; Atahan, A.O. Minimization of Accident Severity Index in Concrete Barrier Designs Using an Ensemble of Radial Basis Function Metamodel-Based Optimization. *Optim. Eng.* **2021**, *22*, 485–519. [CrossRef]
13. Paulsen, G.W.; Faller, R.K.; Reid, J.D. *Design and Testing of a Breakaway Base for a Cluster Box Unit and a Neighborhood Delivery & Collection Unit*; Midwest Roadside Safety Facility, University of Nebraska-Lincoln: Lincoln, NE, USA, 1996.
14. LS-DYNA, Keyword User's Manual. Vol. II. Material Models. 2015. Available online: https://lsdyna.ansys.com/manuals/ (accessed on 2 January 2025).
15. LS-DYNA, Keyword User's Manual. Vol. I. 2015. Available online: https://lsdyna.ansys.com/manuals/ (accessed on 2 January 2025).
16. Vogel, J.C.; Faller, R.K.; Reid, J.D.; Sicking, D.L. *A Review of Breakaway Supports for Small Signs and Mailbox Installations*; Report No. TRP-03-68-98; Texas Transportation Institute: College Station, TX, USA, 1998.
17. Tahan, F.; Marzougui, D.; Zaouk, A.; Bedewi, N.; Eskandarian, A.; Meczkowski, L. Safety Performance Evaluation of Secure Mailboxes Using Finite Element Simulations and Crash Testing. *Int. J. Crashworthiness* **2005**, *10*, 341–349. [CrossRef]
18. Sheikh, N.M.; Bligh, R.P.; Menges, W.L.; Haug, R.R. *Crash Testing and Evaluation of the Shur-Tite® Multiple-Mailbox Mount*; Report No. FHWA/TX-06/0-5210-2; Texas Transportation Institute: College Station, TX, USA, 2006.
19. Bligh, R.P.; Menges, W.L. *NCHRP Report 350 Crash Testing and Evaluation of the S-Square Mailbox System*; Texas Transportation Institute: College Station, TX, USA, 2010.
20. Bligh, R.P.; Menges, W.L.; Sanders, S.K. *Testing and Evaluation of Molded Plastic Mailboxes*; Report No. FHWA/TX-01/1792-6; Texas Transportation Institute, Texas A & M University System: College Station, TX, USA, 2001.
21. Silvestri Dobrovolny, C.; Bligh, R.P.; Obinna, J.; McDaniel, M.; Odell, W. Manual for Assessing Safety Hardware Crash Testing and Evaluation of Multiple Mailbox Supports for Use with Locking Architectural Mailboxes. *Transp. Res. Rec.* **2019**, *2673*, 684–695. [CrossRef]
22. Noureddine, A.; Eskandarian, A.; Digges, K. Computer Modeling and Validation of a Hybrid III Dummy for Crashworthiness Simulation. *Math. Comput. Model.* **2002**, *35*, 885–893. [CrossRef]
23. Deng, X.; Potula, S.; Grewal, H.; Solanki, K.N.; Tschopp, M.A.; Horstemeyer, M.F. Finite Element Analysis of Occupant Head Injuries: Parametric Effects of the Side Curtain Airbag Deployment Interaction with a Dummy Head in a Side Impact Crash. *Accid. Anal. Prev.* **2013**, *55*, 232–241. [CrossRef] [PubMed]
24. Teng, T.L.; Chang, F.A.; Liu, Y.S.; Peng, C.P. Analysis of Dynamic Response of Vehicle Occupant in Frontal Crash Using Multibody Dynamics Method. *Math. Comput. Model.* **2008**, *48*, 1724–1736. [CrossRef]
25. Fang, H.; Li, Z.; Fatoki, O.; Palta, E. Risk Assessment of Roadside Utility Structures Under Vehicular Impacts. Tech Report NCDOT 2018-24. Available online: https://rosap.ntl.bts.gov/view/dot/56016/dot_56016_DS1.pdf (accessed on 30 October 2024).
26. NCAC. Technical Summary—Extended Validation of the Finite Element Model for the 2010 Toyota Yaris Passenger Sedan. Available online: https://media.ccsa.gmu.edu/cache/NCAC-2012-W-005.pdf (accessed on 30 October 2024).

27. NCAC. Technical Summary—Development & Validation of a Finite Element Model for the 2010 Toyota Yaris Passenger Sedan. Available online: https://media.ccsa.gmu.edu/cache/NCAC-2011-T-001.pdf (accessed on 30 October 2024).
28. Li, Z.; Fang, H.; Fatoki, J.; Gutowski, M.; Wang, Q. A Numerical Study of Strong-Post Double-Faced W-Beam and Thrie-Beam Guardrails Under Impacts of Vehicles of Multiple Size Classes. *Accid. Anal. Prev.* **2021**, *159*, 106286. [CrossRef]
29. Wang, Q.; Palta, E.; Fang, H. Numerical Modeling and Simulation of Cable Barriers Under Vehicular Impacts on a Sloped Median. *Int. J. Protect. Struct.* 2024, *in press*. [CrossRef]
30. Fang, H.; Jaus, C.; Wang, Q.; Palta, E.; Pachocki, Ł.; Bruski, D. Numerical Modeling and Simulation of Vehicular Crashes into Three-Bar Metal Bridge Rail. *Computation* **2024**, *12*, 165. [CrossRef]
31. NHTSA. Available online: https://www.nhtsa.gov/crash-simulation-vehicle-models (accessed on 30 October 2024).
32. Li, N.; Fang, H.; Zhang, C.; Gutowski, M.; Palta, E.; Wang, Q. A Numerical Study of Occupant Responses and Injuries in Vehicular Crashes into Roadside Barriers Based on Finite Element Simulations. *Adv. Eng. Softw.* **2015**, *90*, 22–40. [CrossRef]
33. Wang, J.; Nefske, D. A New CAL3D Airbag Inflation Model. *SAE Tech. Pap.* **1988**, *880654*, 697–706. [CrossRef]
34. Hallquist, J. LS-DYNA, Theory Manual. 2006. Available online: https://lsdyna.ansys.com/manuals/ (accessed on 2 January 2025).
35. Florence Corporation. Vital Cluster Box Unit—Type I. Available online: https://www.florencemailboxes.com/sites/default/files/2017-02/1570-8.pdf (accessed on 30 October 2024).
36. Florence Corporation. Vital Cluster Box Unit—Type IV. Available online: https://www.florencemailboxes.com/sites/default/files/2017-02/1570-13.pdf (accessed on 30 October 2024).
37. Hertz, E. A Note on the Head Injury Criterion (HIC) as a Predictor of the Risk of Skull Fracture. In Proceedings of the Association for the Advancement of Automotive Medicine Annual Conference, San Antonio, TX, USA, 4–6 November 1993; Volume 37, pp. 303–312.